Control of a Forward-Swept-Wing Configuration Dominated by Flight Dynamic/Aeroelastic Interactions

M. Rimer,* R. Chipman,* and B. Muniz†
Grumman Aerospace Corporation, Bethpage, New York

An active control system concept for an aeroelastic wind tunnel model of a statically unstable forward-swept-wing configuration with wing-mounted stores is developed to provide acceptable longitudinal flying qualities while maintaining adequate flutter speed margin. On forward-swept-wing configurations, the inherent aeroelastic wing divergence tendency causes strong flight dynamic/aeroelastic interactions that, in certain cases, can produce a dynamic instability known as body-freedom flutter. The carriage of wing-mounted stores is shown to severely aggravate this problem. The control system developed combines a canard-based stability augmentation system with an active divergence/flutter suppression system that relies on wing-mounted sensors and a trailing-edge device (flaperon). Synergism between these two systems is exploited to obtain the flying qualities and flutter speed objectives.

Background

FORWARD-swept wings (FSW) wash in (twist leading edge up) under air-load. From a dynamics viewpoint, the fundamental wing-bending mode can be said to destiffen (drop in frequency) with increasing airspeed. This destiffening or aeroelastic-divergence tendency inherent in the wing can cause strong flight dynamic/aeroelastic interactions on FSW vehicles that, in certain cases, can produce a dynamic instability called body-freedom flutter (BFF).[1-3] Emerging FSW technology[4,5] has demonstrated that, by proper aeroelastic tailoring using advanced composite materials, the basic aeroelastic divergence behavior of the wing can be delayed and/or reduced. Thus, the speed at which BFF would occur can be increased. There are limits beyond which this design approach is neither practical nor desirable. For example, tailoring the wing to be stiff enough to avoid BFF in all of a variety of store loadings can be weight prohibitive and, at best, will penalize the clean-wing design unduly. A better approach is to employ aeroelastic tailoring for the clean-wing configuration and develop an active concept to enable stores to be carried without flutter speed restriction.

In prior work,[1,2] a concept was introduced for this active divergence/flutter suppression (ADFS) task. A conceptual divergence/suppression system architecture was described[1] for a simplified FSW clean-wing configuration. This work was expanded[2] to a realistic tactical configuration with wing-mounted stores. In the present paper, the concept is adapted to a ½-scale aeroelastic wind tunnel model of a statically unstable FSW configuration with wing-mounted stores. First, a canard-based stability augmentation system (SAS) is designed to provide longitudinal stability for the clean-wing configuration. Next, an ADFS system is added to prevent BFF on the full-up (stores added) configuration. The focus is on achieving acceptable longitudinal flying qualities while providing the required flutter speed margin. The flying qualities question is addressed via several current evaluation techniques. These include the Control Anticipation Parameter (CAP),[6] Equivalent Systems Response,[7] Implict Model Following, and time history *g*-response at the pilot station. The full-up configuration is characterized by very strong coupling between the wing-bending and aircraft short-period modes. Attainment of both the desired aeroelastic and flight dynamic characteristics is shown to require the synergistic combination of the SAS and ADFS system.

This paper is organized in the following manner. First, descriptions of the wind tunnel model (plant) and its various mathematical idealizations (e.g., aerodynamic and dynamic) are given. These are followed by reviews of the clean-wing SAS design and a wind tunnel demonstration of its performance. Next, analytical predictions of the effect of store carriage on the BFF are presented. Finally, the design and analytical evaluation of the ADFS are presented,, including the assessment of flying qualities.

Wind Tunnel Model and Its Idealizations

The wind tunnel article on which this study is based is a statically unstable, ½-scale, semispan aeroelastic FSW model that was successfully flown in August 1983 on a cable-support system in the NASA Langley 16 ft Transonic Dynamics Tunnel. A clean-wing (no stores) configuration was tested using the SAS described herein to supply longitudinal stability. Details of that test program have been documented.[8] Figure 1 shows the configuration and Table 1 presents the relevant data. For the present study, a wing-tip and an under-wing-mounted store are considered to be attached to the wing via rigid pylons and launchers. These stores are scaled versions of Sidewinders—an armament compatible with a fighter FSW configuration.

Comprehensive dynamic and aerodynamic (both steady and unsteady) idealizations of the model with wing-mounted stores were developed (Fig. 2). The clean-wing idealization was consistent with the existing cable-supported wind tunnel model and included the canard-based SAS designed for that test. For simplicity, the dynamics of the cable support system were omitted in the present study. Using a symmetric free-free dynamics idealization, the rigid-body modes (pitch and plunge) and four flexible modes were computed by mass coupling the stores to a set of clean-wing modes measured on the existing model. For the SAS, an accelerometer and pitch

Presented as Paper 84-1866 at the AIAA Guidance and Control Conference, Seattle, WA, Aug. 20-22, 1984; submitted Sept. 12, 1984; revision received Feb. 15, 1985.

*Engineering Specialist. Member AIAA.
†Associate Engineer. Member AIAA.

rate gyro mounted at the aircraft's center of gravity were used as sensors. The SAS block diagram is shown as part of Fig. 3. For the ADFS function, two additional accelerometers are assumed to be added: one near the wing tip just forward of the flaperon leading edge and one at the wing root at the same station. From these two sensors, relative wing motion is detected. The ADFS block diagram is also shown in Fig. 3 as a wraparound to the basic SAS.

A state-variable representation of the system incorporating the aerodynamic, elastic, and inertial terms from the above idealizations was formulated using the SAEL code.[1,8] The resulting equation can be symbolically abbreviated as

$$\begin{bmatrix} \dot{x}_r \\ \dot{x}_f \\ \dot{x}_c \end{bmatrix} = \begin{bmatrix} A_{rr} & A_{rf} & A_{rc} \\ A_{fr} & A_{ff} & A_{fc} \\ 0 & 0 & A_{cc} \end{bmatrix} \begin{bmatrix} x_r \\ x_f \\ x_c \end{bmatrix} + \begin{bmatrix} 0 \\ 0 \\ B_c \end{bmatrix} u \qquad (1)$$

where the subscript r denotes the rigid-aircraft states, subscript f the flexible (modal) states, and subscript c the controller states (actuators, integrators, etc.). In the clean-wing SAS design process, the flexible states are not considered and, consequently, the rigid aerodynamic coefficients are scaled to match the corresponding total (flexibilized) values. Also, only the canard is included in the u vector. For the purpose of investigating BFF and the effect of stores, the full state variable representation given in Eq. (1) is used. In the design and evaluation of the ADFS, the complete representation is used with both canard and flaperon present. Sensor dynamics, pilot stick dynamics, and a command generator also are included.

Clean-Wing SAS Design

The architecture of the g-command longitudinal control system includes a pitch rate gyro and an N_z accelerometer to sense model motions, and a canard actuator driven by a combination of proportional plus integral compensation. The pitch rate feedback q provides system damping, while the forward loop integrator eliminates steady-state errors. Additionally, a positional command (directly to the actuator) is added for trimming the model. With this system, and the stick in detent, the model will maintain 1-g flight independent of airspeed. At constant airspeed, a step stick input will result in a constant time rate of change of flight path angle $\dot{\gamma}$; a pulse will result in an incremental change in the flight path angle $\Delta\gamma$.

An algebraic synthesis technique[9] was used to design the basic rigid-body Flight Control System. By neglecting the actuator dynamics and placing the zero provided by the proportional plus integral compensation at the stable open-loop model pole location, the following approximate transfer function may be written:

$$\frac{\Delta N_z(S)}{\Delta N_{z_c}(S)} = \frac{G}{S^2 + 2\xi_{sp}\omega_{sp}S + \omega^2{}_{sp}} \qquad (2)$$

where G, ξ_{sp}, and ω_{sp} are functions of the plant characteristics, the control system gains K_F, K_I, K_{N_Z}, and K_Q, and the airspeed. Treating ξ_{sp} and ω_{sp} (closed-loop short-period damping and frequency) as parameters and constraining G so as to yield zero steady-state error, expressions can be derived for the control system gains required to yield the desired pure second-order short-period response. A typical pole-zero configuration is shown in Fig. 4 along with the resultant gain root locus. The locus is seen not to pass directly through the design goal since, for evaluation purposes, the actuator dynamics are now included.

Table 1 Configuration data

Data (½ airplane)	Model
Mass	10 slugs
Pitch inertia	324 slug-ft^2
Semispan	6.8 ft
Semichord	3.6 ft
Wing area (to centerline)	22.8 ft^2
Wing leading-edge sweep	−29.3 deg
Canard area	2.6 ft^2
Static margin	−25%
Design point	$M=0.9$, sea level
Wind tunnel design point	$M=0.9$, $Q=83$ lb/ft^2

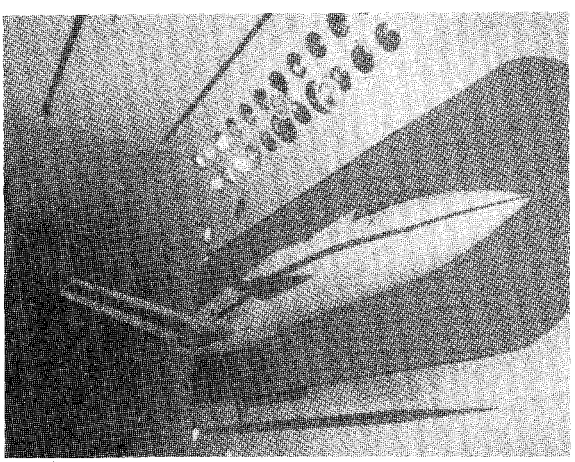

Fig. 1 One-half scale FSW aeroelastic model installed in NASA Langley Transonic Dynamics Tunnel.

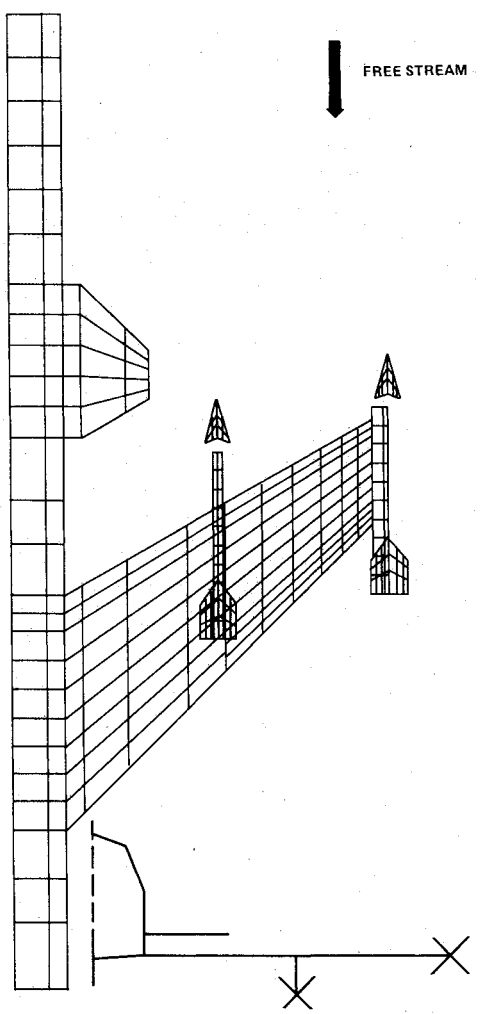

Fig. 2 Aerodynamic idealization of an aeroelastic FSW model with wing-mounted stores.

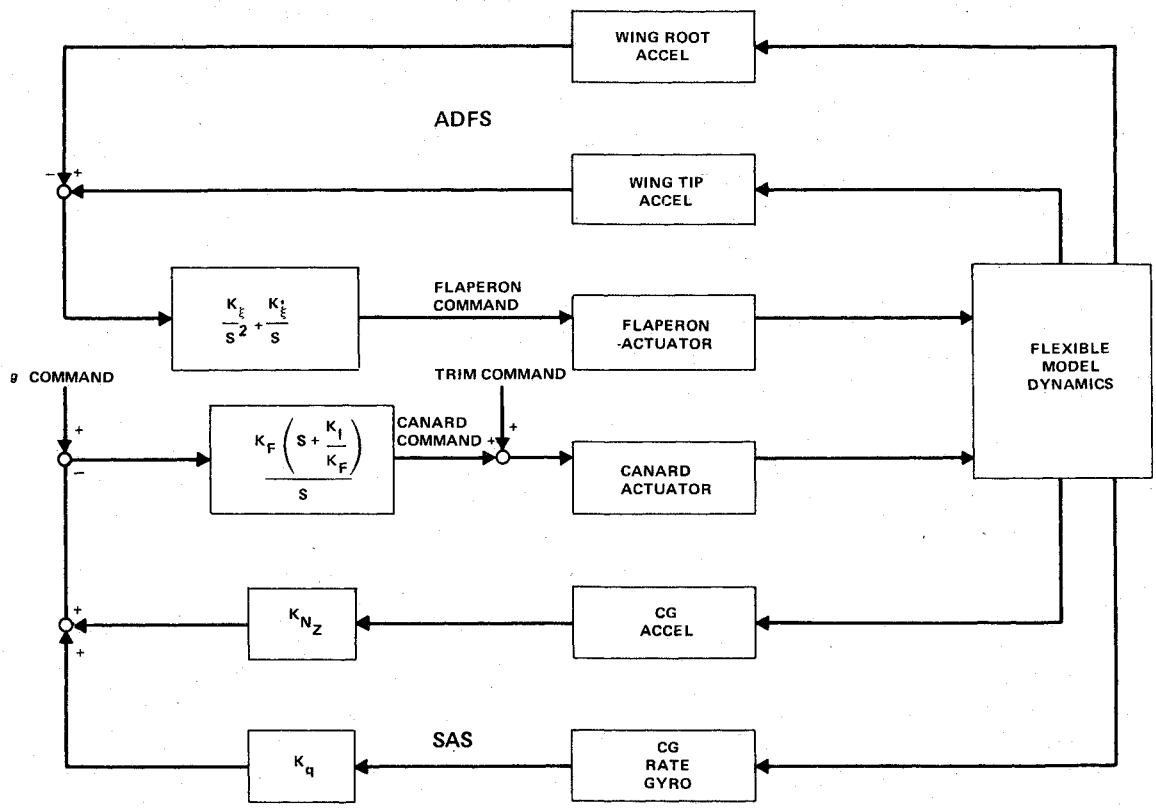

Fig. 3 System block diagram.

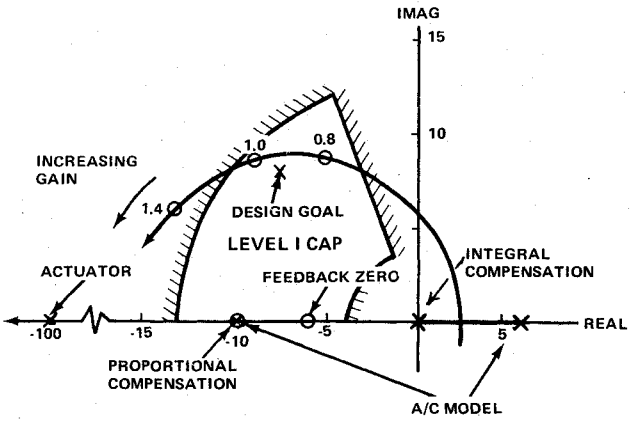

Fig. 4 Typical gain root locus.

The design goal was derived using the CAP as the response metric. CAP relates the initial aircraft pitch acceleration to the steady-state normal load factor and forms the basis of the primary specification on short-period flying qualities.[6] For conventional statically stable aircraft, CAP is defined in the context of a step input to the elevator (or canard). For a statically unstable aircraft such as considered here, this definition is inappropriate because the surface must have the freedom to move incrementally to maintain the stability (i.e., to prevent aircraft departure). Consequently, the definition is modified to reflect response to a step input to the stick not the surface itself. With this modification implicit in the definition of CAP, the following relationship is assumed:

$$\omega^2_{sp} = \mathrm{CAP} \cdot N_{z_\alpha} \tag{3}$$

Thus, the design goal in CAP is converted to a desired short-period frequency. To complete the specification of the design goal, a damping ratio ξ is selected.

To make the model test configuration relevant to current FSW aircraft development, CAP and ξ were chosen to be representative of real aircraft at atmospheric conditions equivalent to the wind tunnel flight conditions. In particular, CAP and ξ were specified as midrange of level I flying qualities for category A flight phase. In Fig. 4, these goals are indicated together with the level I upper and lower limits on CAP and the lower limit on the damping ratio, translated from MIL-F-8786C. (The military specification of the upper damping limit is over-critically damped.)

Wind Tunnel Demonstration of Clean-Wing SAS

The final design of the control laws tested was based on aerodynamic data measured on the model in an initial wind tunnel entry,[8] as well as on measurements of the model's mass and flexible properties. A demonstration of the SAS performance made during the subsequent tunnel entry included as direct verification of its ability to stabilize an otherwise unstable configuration.

Figure 5 documents the SAS verification. Three traces are shown: fuselage N_z acceleration, fuselage pitch rate, and canard command. The test configuration had a moderately unstable static margin (-10% unstable); the flight condition was $M=0.86$, $Q=58$ lb/ft^2. As the trace begins, the model is trimmed and flying. At the point indicated, the SAS is turned off. Within 1 s the model can be seen to oscillate; within 2 s the motion was rapidly diverging. At 3.5 s the SAS was re-engaged and, as seen, the oscillations quickly subsided. (It should be explained that, although on a freely flying aircraft departure would have occurred when the SAS was turned off, on the wind tunnel model the oscillatory behavior observed was to be expected. This difference is due to the influence of the cable-support system.)

BFF and Effect of Stores

Using the SAEL (Servo Aero Elastics) code,[8] a comprehensive state-variable representation of the flexible model was created [Eq. (1)] and root loci at varying dynamic pressures were generated for the SAS alone (no ADFS) for both the clean-wing and wing/stores configurations. Figure 6 shows these loci. For simplicity, only the short-period and primary wing bending modes are plotted. The classic interaction of two modes producing BFF is evident for both configurations. The sea level match points and the BFF instability points marked thereon indicate that, whereas the clean-wing configuration has ample speed margin (51% in dynamic pressure, 23% in speed), the wing/stores case does not (−24% in dynamic

pressure, −13% in speed) and is even unstable at the design condition. This dramatic decrease in stability due to the presence of wing-mounted stores presents a substantial challenge to the ADFS. It should be noted that, for the stores case, the frequencies of the wing mode and short-period mode are in very close proximity at the design point, further complicating the challenge.

ADFS Design

The ADFS design was accomplished using the novel synthesis concept developed[2]—an extension of the optimization technique known as implicit model-following to a representation of flexible model dynamics as well as rigid-body dynamics. In particular, linear quadratic output-state-feedback optimization was employed using the CASCADE (Computer-Aided Synthesis Computer-Aided Design Evaluation) operating system.[10] Two implicit models were formulated to drive the design, i.e., a model for the longitudinal flying qualities and a separate model of the wing bending dynamics. Both implicit models were based on the clean-wing dynamics at the design point. The design condition was the wing/stores configuration at $M=0.9$, sea level, and the goals were: 1) +15% speed margin against BFF, 2) recovery of the clean-wing flying qualities (short-period frequency and damping) at the design point, and 3) moderate flaperon displacement (± 10 deg) but relaxed rates (up to 80 deg/s).

The design problem is to develop a SAS and an ADFS control system that approximate the responses of the second-order systems (i.e., the implict models) with specified bandwidth and damping. The "optimization" to be performed involves determination of the six controller parameters/gains K_q, K_{N_z}, K_1, K_F, K_ξ, and $K_{\dot{\xi}}$. The augmented state vector equation,

$$\dot{X}=AX+BU \tag{4}$$

contains all of the system transfer functions including the flexible model [Eq. (1)] of the plant, the implicit models, and a pulse command generator to excite the plant and implicit models. The error vector Y used in the performance index can be represented as a linear combination of the state vector X and the control vector U, i.e.,

$$Y=CX+HU \tag{5}$$

It is noted that the Y vector can be defined in terms of variables or elements of X that might not necessarily be measurable in the real world. The optimization accommodates this freedom by constraining the solution to apply gains only to elements that are physically realizable numbers in the flight control system computer as defined by the measurement vector Z, i.e.,

$$Z=EX \tag{6}$$

The output feedback solution will try to minimize the Y characterization of the performance index J,

$$J=\int_0^\infty (Y^tQY+U^tRU)\mathrm{d}t \tag{7}$$

but only to the extent that feeding back elements of Z will permit. Finally, the control vector U is formed by the product of the gain matrix and Z, i.e.,

$$U=D_zZ \tag{8}$$

For the problem at hand, the error vector Y was chosen to consist of five elements: the errors in aircraft vertical acceleration, aircraft pitch rate, aircraft pitch acceleration, relative wing-tip displacement, and relative wing-tip rate. Each error was defined as the difference between the implicit model variable and the respective aircraft variable, e.g.,

$$y_1=N_z(\text{implicit model})-N_z(\text{aircraft}) \tag{9}$$

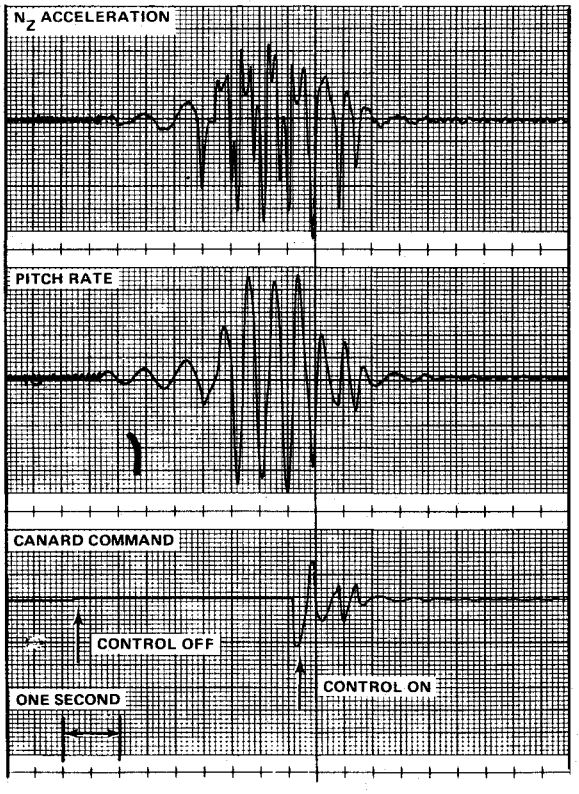

Fig. 5 Verification of SAS function.

The measurement vector was comprised of five elements: aircraft vertical acceleration, aircraft pitch rate, output from the forward-path integrator, relative wing-tip displacement, and relative wing-tip rate. The control vector consisted of inputs to the canard and flaperon.

Attempts were made to obtain a satisfactory design with gains on the first three measurements held fixed at their clean-wing SAS values. Due to the close coupling of the short-period and wing-bending dynamics, this approach was not successful. To help comprehend this result, a gain root locus was generated for the wing/stores case, varying only the gains on the relative wing displacement and rate (K_ξ and $K_{\dot{\xi}}$). Figure 7 shows this plot. The desired short-period root is marked by an X; the desired wing-bending is essentially as high in frequency and damping as can be obtained. The solid curve corresponds to zero rate gain and varying displacement gain. As can be seen, stability of the wing-bending mode is obtained at the expense of short-period damping and frequency, and low levels of the wing-bending damping are exhibited for all gains. The L1 set of dashed curves indicates that further attempts to increase the damping and frequency of the wing-bending mode by raising rate gain lead to a further deterioration of the short-period. Dashed curves L2 and L3 indicate that, for certain combinations of rate and displacement gains, the character of the wing-bending and short-period modes can interchange. Thus, it may be seen that no combination of these two gains alone results in both the desired short-period mode and a stable wing-bending mode.

Following the lack of success in the three-fixed-gain approach, attention turned to determining five gains simultaneously. To achieve the solution to this multi-input/multi-output (MIMO) output state feedback optimization problem, quadratic weights (Q and R) were assigned in the performance index to the five elements of the error vector and two elements of the control vector. By varying these weights, a number of candidate designs were obtained using the CASCADE optimization code. Velocity loci were generated for the most promising of these designs. Two of these (denoted C36 and C70) were judged worthy of more

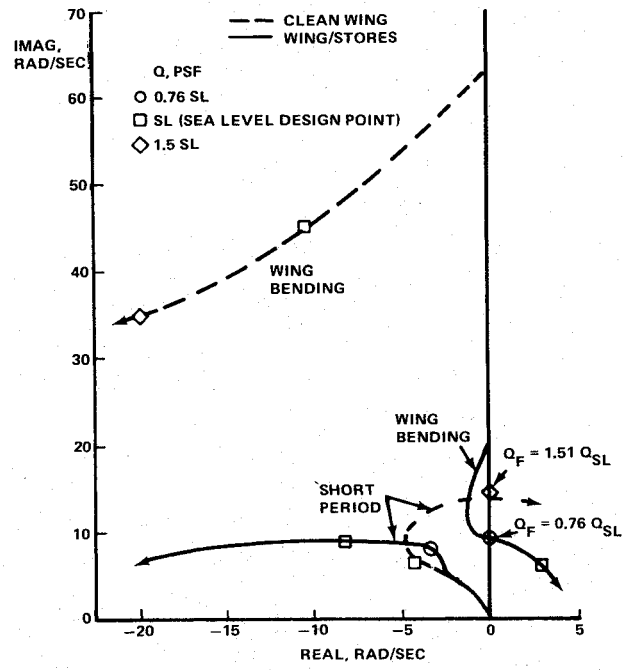

Fig. 6 Root loci for clean-wing and wing/stores configuration, SAS alone (no ADFS).

detailed evaluation. The corresponding velocity loci are shown in Fig. 8. Both designs raise the BFF speed margins significantly and, as can be seen, C70 is the better design in terms of BFF speed margin (19%). Compared to the SAS-only (no ADFS) case, this represents a remarkable 87% increase in dynamic pressure. Note that the optimization was able to place the short-period mode reasonably close to its design goal (marked by an X), while simultaneously raising the wing-bending frequency.

To obtain an estimate of the control requirements in a turbulent environment, a set of time responses was generated at the design velocity for a 1 ft/s impulsive wing-tip rate, simulating an abrupt gust. Figures 9 and 10 highlight these results for C36 and C70. C70 shows the wing-bending mode to be lowly damped; consequently, its control rates remain relatively high. On the other hand, C36 quickly damps out the disturbance and the control demands diminish accordingly. At this point, there is very little to choose from between the two designs, but a further investigation (described below) will show C70 to be superior.

Flying Qualities Assessment

For each of the two designs, the increase in BFF speed margins is obtained mainly because the short-period dynamics have been separated from the wing-bending mode frequency. For control law C70, the locations of the short-period and wing modes at the design velocity are $-6.6 \pm 8.0i$ and $-1.0 \pm 15.4i$, respectively; while for C36 they are $-4 \pm 4i$ and $-13 \pm 17.5i$(Fig. 8). Both designs led to significant increases in the flutter speeds. It can be seen that the short-period roots of both designs fall within level I flying qualities boundaries but, because many of the dynamic modes are closely coupled (particularly the short-period and the first wing-bending), the evaluation of the flying qualities requires more than just representing the aircraft by its predominant second-order roots. As a first cut, the flying qualities were judged via comparisons of the vertical acceleration N_z and the pitch rate time responses with their respective implicit models. The same pulse input used for synthesis purposes was applied for this evaluation. Figures 11 and 12 illustrate how the two designs perform relative to the implicit models (N_z, q), as well as the demands on the control surfaces' displacements and rates.

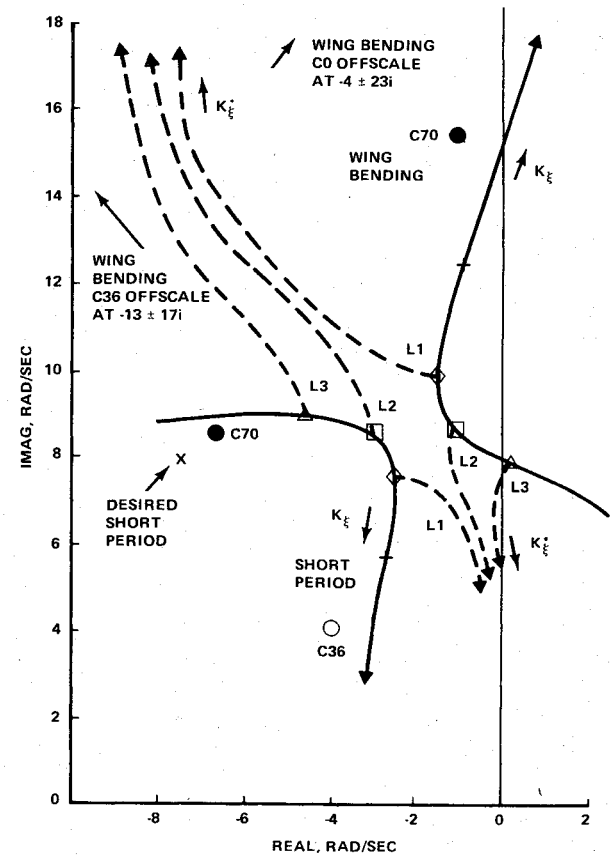

Fig. 7 Gain root loci for K_ξ and K_ξ.

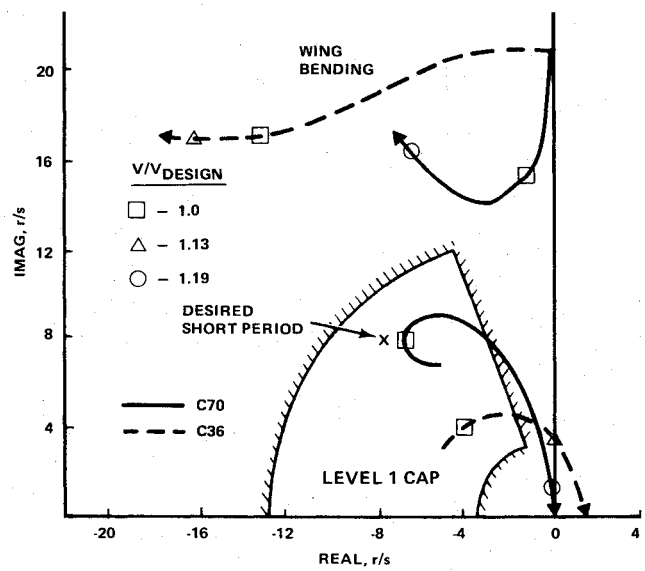

Fig. 8 Velocity loci for ADFS designs C36 and C70.

Figure 11 shows the aircraft acceleration and pitch rate responses to the pulse N_z command. The top plots compare C36 to the implicit model; the bottom plots compare C70 to the implicit model. C36 tracks pitch rate very accurately, but lags in acceleration; C70 tracks acceleration very accurately, but overshoots the desired pitch rate. Figure 12 shows the flap and canard deflections and rates for C36 (top) and C70 (bottom).

MIL-F-8785C[6] prescribes the use of the equivalent systems approach to assess flying qualities. This approach utilizes fre-

quency response matching techniques to determine low-order transfer functions that approximate the response of the actual high-order system. When the scope of this representation is restricted to the determination of short-period characteristics, the desired form of the low-order system transfer function relating pitch rate q to stick force is

$$\frac{q}{\delta_{ST}} = \frac{K_1 e^{-\tau_{qe}}(s + 1/\tau\Theta)}{s^2 + 2\zeta_e\omega_e s + \omega_e{}^2} \tag{10}$$

The five parameters in the function are the pitch rate gain K_1, equivalent pitch rate time delay τ_{qe}, numerator time constant τ_θ, equivalent short-period damping ζ_e, and equivalent short-period frequency ω_e. Two of these parameters directly relate to the flying qualities criteria, i.e., ζ_e and τ_{qe}. From the parameter ω_e, another flying qualities parameter (CAP) can be computed. It has also become common practice to obtain an equivalent system representation by matching Eq. (10) to the actual transfer function of pitch rate to stick force, while simultaneously matching the following equation to the actual transfer function of normal acceleration to stick force:

$$\frac{N_z}{\delta_{ST}} = \frac{K_2 e^{-\tau}Ne}{s^2 + 2\zeta_e\omega_e s + \omega_e^2} \tag{11}$$

In this case, two additional matching parameters arise, the N_z gain K_2 and the equivalent N_z time delay τ_{Ne}. Both single and simultaneous matches were obtained for the two designs, C36 and C70.

Flying quality parameters obtained from these equivalent systems matches are shown in Fig. 13, where the level I, II, and III regions for the category A flight phase[6] are indicated. Four results are shown for each design. First, the q-match results are examined. There is controversy in the literature[7] over whether it is appropriate to set $1/\tau_\theta$ equal to the airplane's L_α or to allow the matching algorithm to compute a best value (albeit, nonphysical) for the match. For the designs, Fig. 13 shows that both approaches gave essentially the same results; both designs have level I flying qualities, although the short-period damping for C36 is marginally level I. From the simultaneous-match results, it can be seen that they differ from their single-match counterparts; however, design C70 still receives a level I rating. On the other hand, design C36 shows an anomaly, i.e., the N_z-equivalent time delay is quite different from the q-equivalent time delay and, in fact, lies in the level II area. Furthermore, the mismatch parameters arising from these fits indicate that C36 is more poorly matched by its equivalent system than is C70. These findings suggest that C36 is a nonstandard higher-order system and, thus, would be less acceptable to pilots than C70.

Another technique—examination of the g-response at the pilot station—was used to further compare the two designs. This approach is somewhat subjective in that it relies on a judgment of what g-response trends pilots would like to feel in flying the airplane. On a stable aircraft with elevator control, the typical pilot station response increases monotonically with time, has its steepest slope at time zero, and asymptotically reaches its steady-state commanded g level. On an unstable aircraft with canard control, the initial reaponse tends to be quite different. Because the canard is very effective in initiating the maneuver, the initial slope of the response is very steep, i.e., the response is said to "jump off" at time zero. Because the configuration is unstable, the canard then has to reverse its deflection to recover the aircraft, thus causing a subsequent undesirable reduction or "pullback" in the response. Thereafter, the response curve traces a traditional monotonic increase asymptotically to the commanded g-level. Figure 14 shows the pilot station g-response for designs C36 and C70. For C36, the initial jumpoff is followed by a drastic pullback. It is easily envisioned that such a pullback might induce a pilot to command additional g's. Thus, this response

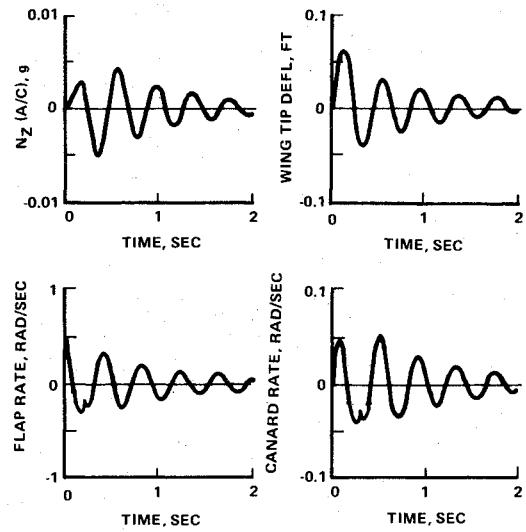

Fig. 9 ADFS (C70) responses and control motions after a 1.0 ft/s wing-tip impulse.

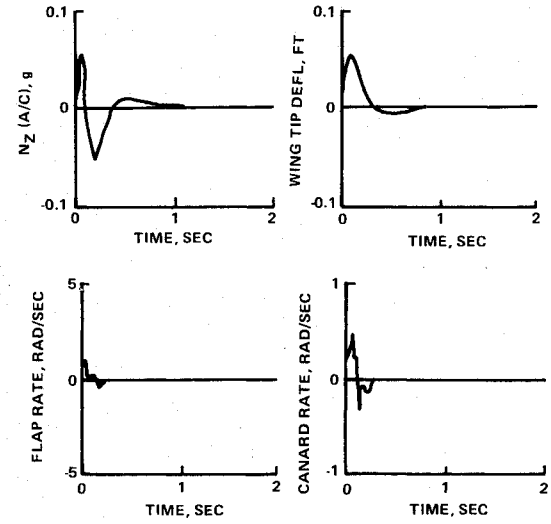

Fig. 10 ADFS (C36) responses and control motions after a 1.0 ft/s wing-tip impulse.

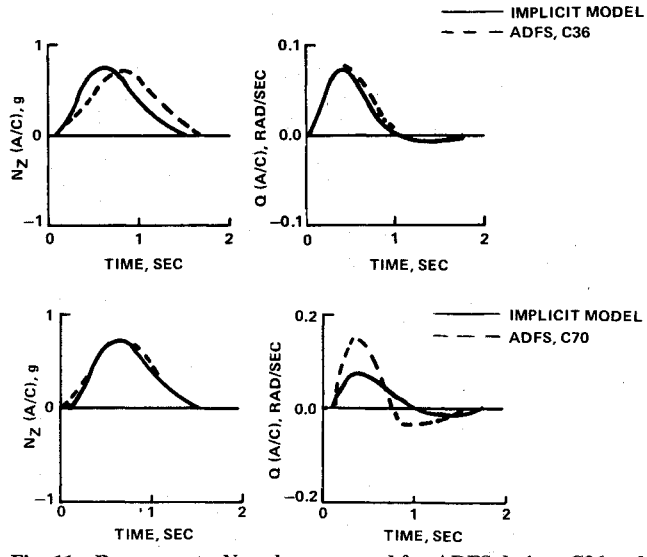

Fig. 11 Responses to N_z pulse command for ADFS designs C36 and C70.

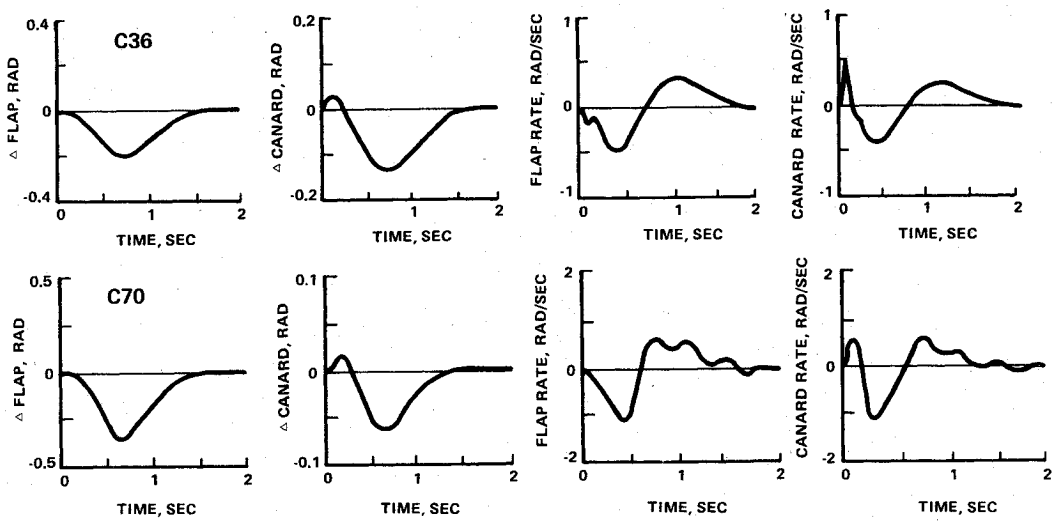

Fig. 12 Control displacements and rates for N_z pulse: ADFS designs C36 and C70.

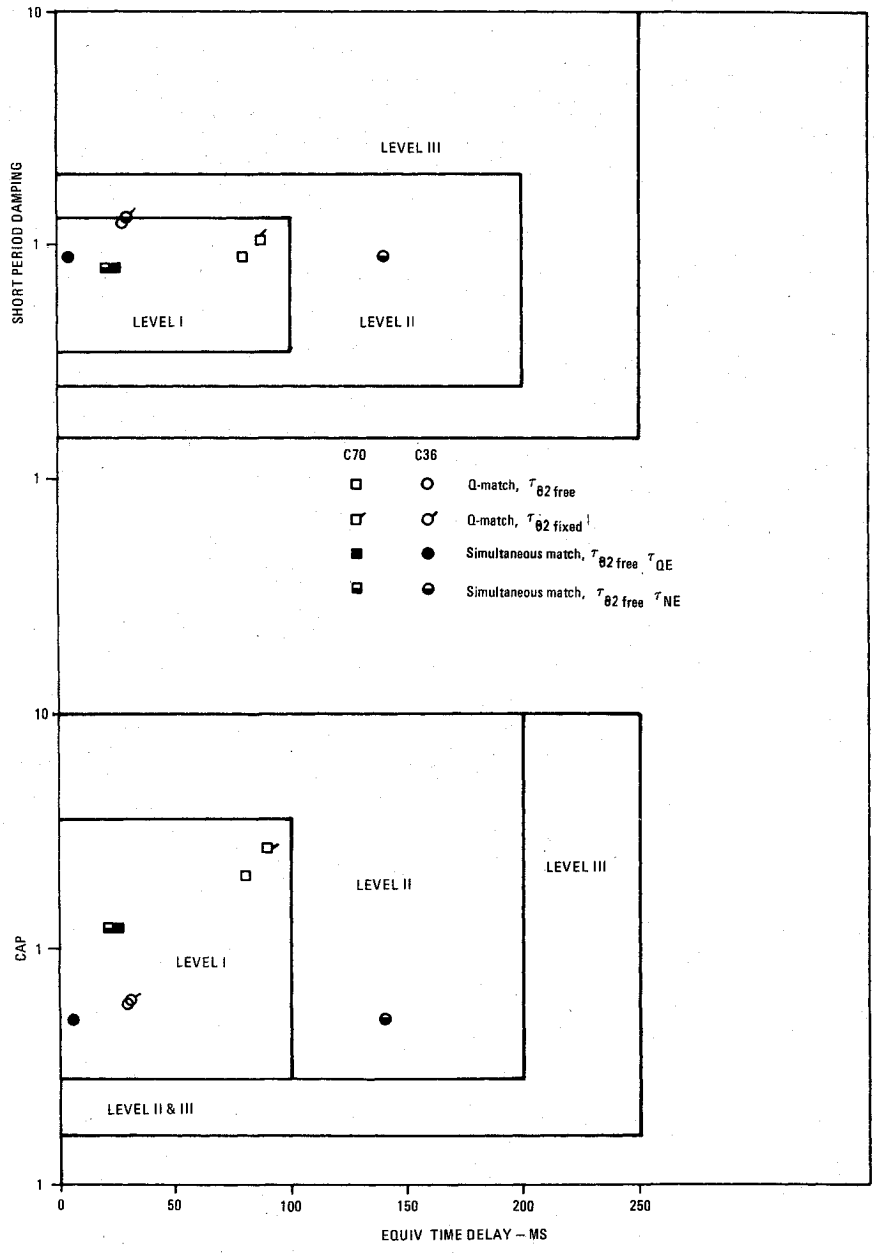

Fig. 13 Equivalent systems flying qualities.

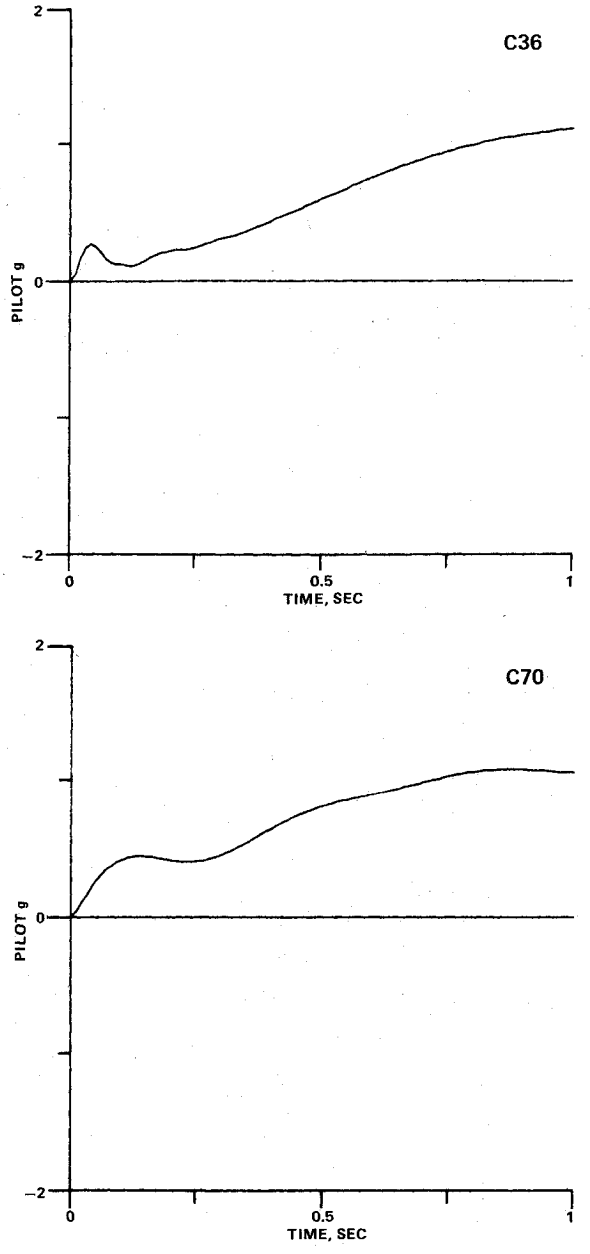

Fig. 14 *g*-response at pilot station.

curve is prone to result in overcommanding the aircraft and, hence, control design C36 would undoubtedly receive a poor pilot rating. On the other hand, C70 exhibits a much less drastic pullback and, consequently, would receive a far superior pilot rating, which is consistent with the equivalent systems results.

From the various assessments discussed above, it is concluded that the C70 design is superior to C36 and is acceptable from a flying qualities perspective. However, it is recognized that the ultimate judge of flying qualities is the pilot and that piloted simulations and/or piloted vehicle tests are necessary to prove out such a nonstandard system.

Conclusions

The impact of body-freedom flutter on control system design for a forward-swept-wing model with wing-mounted stores has been studied. Designs were developed that not only stabilized a forward-swept-wing configuration exhibiting high relaxed static stability, but also provided adequate speed margin against body-freedom flutter. The synthesis process used output-state linear quadratic optimal control theory and employed implicit models of both the desired flying qualities and the flexible modal dynamics. Candidate designs were evaluated on the basis of flutter speed margin and assessments of longitudinal flying qualities. A variety of approaches were employed in the flying qualities assessment: parameter constraints (e.g., Control Anticipation Parameter), desired time response, frequency responses, etc. The synthesis and evaluation process demonstrated that a successful strategy in design of an active divergence/flutter suppression system must increase (stiffen) the wing frequency while retaining the desired short-period dynamics. Using the control architecture postulated, this strategy was shown to be entirely feasible. By allowing the synthesis procedure to adjust some of the gains in the original stability augmentation system, while computing gains for the active divergence/flutter suppression system, a combined design was obtained that successfully implemented the strategy to produce a system that attained both the desired flying qualities and flutter speed margin.

Acknowledgment

Portions of this work were supported by NASA Contract NAS1-17102.

References

[1]Chipman, R., Zislin, A., and Waters, C., "Active Control of Aeroelastic Divergence," AIAA Paper 82-0684, May 1982.

[2]Rimer, M., Chipman, R., and Mercadante, R., "Divergence Suppression System for a Forward Swept Wing Configuration with Wing-Mounted Stores," AIAA Paper 83-2125, Aug. 1983.

[3]Miller, G., Wykes, J., and Brosnan, M., "Rigid Body-Structural Mode Coupling on a Forward Swept Wing Aircraft," AIAA Paper 82-0683, May 1982.

[4]Wilkinson, K. and Rauch, F., "Predicted and Measured Divergence Speeds of an Advanced Composite Forward Swept Wing Model," AFWAL-TR-80-3059.

[5]Spacht, G., Calandra, J., et al., "Forward Swept Wing Demonstrator Technology Integration and Evaluation Study," AFWAL-TR-80-3145, Vol. III, Dec. 1980.

[6]Military Specification Flying Qualities of Piloted Airplanes, MIL-F-8785C, Nov. 1980.

[7]Bischoff, D.E., "The Definition of Short-Period Flying Qualities Characteristics via Equivalent Systems," AIAA Paper 81-1775, Aug. 1981.

[8]Chipman, R., et al., "FSW Body-Freedom-Flutter Model Test," NASA CR-172324, April 1984.

[9]Lapins, M., et al., "Control Deflection Study for Advanced Vehicles," NASA CR-3738, Nov. 1983.

[10]Grant, R., "User Data Package for Interim CASCADE Program," Grumman Aerospace Co., Bethpage, NY, Rept. EG-FC-83-39, Oct. 1983.

[11]Smith, R. and Bailey, R., "Effect of Control System Delays on Fighter Flying Qualities," AGARD-CP-333, June 1982.